Protection and Conservation of Georgian Rupestrian Cultural Heritage Sites: A Review

William Frodella, Giovanni Gigli, Daniele Spizzichino, Claudio Margottini, Mikheil Elashvili, and Nicola Casagli

Abstract

Many of the Georgian cultural heritage sites consist of rupestrian monastic complexes constructed between the sixth and the 12th centuries of exceptional universal value from a historical, cultural, and natural point of view. Many of them are affected by hydrogeological problems and require the planning of an effective risk mitigation strategy. This planning would help not only to preserve invaluable cultural heritage sites but also to enhance Georgia as an important tourist destination and improve the local economy. This paper aims to show an overview on the last decade's activities coordinated by the National Agency for the Preservation of Georgian Cultural Heritage (NAGPCH) for the conservation of Georgian cultural heritage, thanks to the collaboration between national and international centers of research.

Keywords

Landslides · Cultural heritage · Remote sensing · Mitigation

W. Frodella (✉) · G. Gigli · N. Casagli
Department of Earth Sciences, University of Florence, Florence, Italy
e-mail: william.frodella@unifi.it; giovanni.gigli@unifi.it

D. Spizzichino
ISPRA, Higher Institute for Protection and Environmental Research, Rome, Italy
e-mail: daniele.spizzichino@isprambiente.it

C. Margottini
UNESCO Chair on Prevention and Sustainable Management of Geo-Hydrological Hazards, University of Florence, Florence, Italy
e-mail: claudio.margottini@unifi.it

M. Elashvili
Ilia State University, Tbilisi, Georgia
e-mail: mikheil_elashvili@iliauni.edu.ge

1 Introduction

Rock-hewn cultural heritage sites are often developed in slopes formed by weak rocks, such as tuffs or soft sandstones, which are characterized by peculiar lithological, geotechnical, and morpho-structural features. These features lead to an excellent carvability, but at the same time, to weathering, deterioration and landsliding. In this context combining traditional approaches (field surveys and laboratory analyses on rock/soil samples) with close-range non-destructive techniques, can profitably be used for the rapid detection of conservation issues that can lead to slope instability phenomena. These phenomena in particular not only can damage the site, but also put visitors at high risk.

The proposed approach can provide fundamental data to implement a site-specific and inter-disciplinary approach for the sustainable protection and conservation of such fragile cultural heritage sites. This paper presents this methodological approach for several important cultural heritage sites of the UNESCO Tentative List, such as Vardzia, Vanis Kvabebi, Uplistsikhe, and David Gareja (Fig. 1). These are located in mountainous areas, river valleys, and half deserts. The final aim is to provide conservators, practitioners, and local authorities with a useful, versatile, and low-cost methodology, to be profitably used in the protection and conservation strategies of rock-carved sites with similar geomorphological and geological characteristics.

1.1 Vardzia and Vanis Kvabebi

The rock-cut city of Vardzia and the rupestrian monastery of Vanis Kvabebi, dating between the eighth and 12th centuries, are carved in the volcanic tuffs of the Erusheti mountains to the north, and the Javaheti plateau to the south (southern Georgia; Fig. 1b). These sites outcrop along the steep slopes of the Mtkavri river gorge, and are formed by the Goderdzi Formation: an Upper Miocene to Lower Pliocene subaerial

I. Alcántara-Ayala et al. (eds.), *Progress in Landslide Research and Technology, Volume 2 Issue 1, 2023*,
Progress in Landslide Research and Technology, https://doi.org/10.1007/978-3-031-39012-8_14

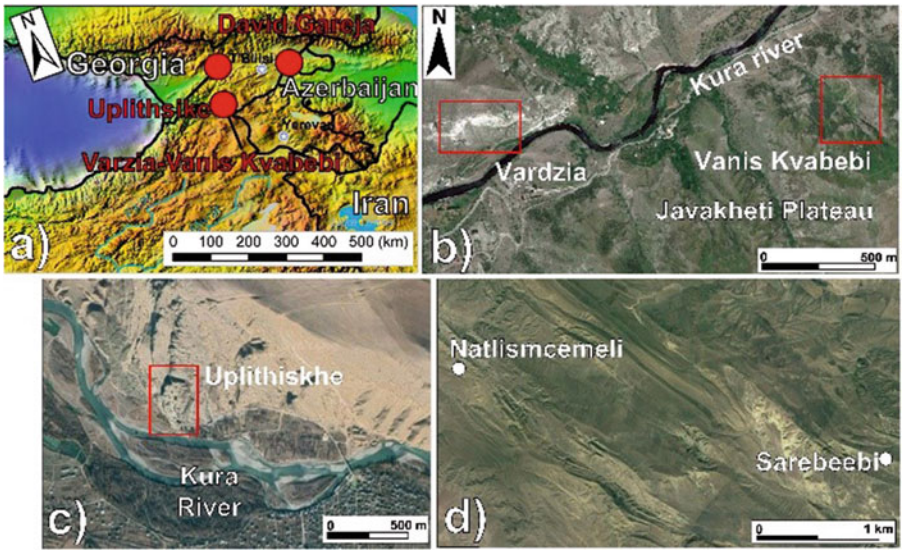

Fig. 1 Map with the location of the analysed rock-carved cultural heritage sites (**a**); locations at a higher scale: (**b**) Vardzia-Vanis Kvabebi; (**c**) Uplithsike; (**d**) David Gareja

volcanogenic–sedimentary sequence, about 1000 m in thickness, composed of volcanic breccias (Layer 1 and 4), and tuffs (Layer 2 and 3) with ashfall deposits (Gudjabidze and Gamkrelidze 2003; Margottini et al. 2015; Okrostsvaridze et al. 2016; Boldini et al. 2018; Frodella et al. 2020a).

1.2 Uplistsikhe

Uplistsikhe is an ancient cave town-fortress located in eastern Georgia about 50 km NW of Tbilisi (Fig. 1c). From a morphological point of view, the complex is located on the left bank of the Kura River on the slopes of the Kvernaqi range. The site develops on top of a rocky terrace bordered to the south-west by a rock cliff up to 40 m high and is completely carved into a thick sequence of Upper Oligocene to lower Miocene quartz coarse sandstones, gently dipping towards SE (Stinghen 2011; Frodella et al. 2021.

1.3 David Gareja

The David Gareja monastery complex is located in Kakheti half-desert region (Eastern Georgia), near the border with Azerbaijan (Fig. 1d). From a geological point of view, the area is formed by a thick sequence of soft sedimentary rocks (Lower Miocene to Pliocene in age) characterized by a monocline "hogback type" structure, with strata dipping SW with low-gentle angles, from very coarse-grained, pebbly thick-bedded sandstones, to coarse-grained soft sandstones, siltstones, and clays (Frodella et al. 2020b, 2021).

2 Materials and Methods

A methodology was implemented integrating field surveys, close-range remote sensing (namely InfraRed Thermography = IRT and Unmanned Aerial Vehicle Digital Photogrammetry = UAV-DP), and laboratory analyses for geotechnical-mineralogical and geological characterization (Fig. 2). The analysis of remote sensing data allowed us to obtain high-resolution slope 3D surfaces and surface temperature maps, while water runoff patterns were mapped in a GIS environment (ESRI 2019). A final phase of data integration and interpretation provided the detection of potential criticalities with respect to weathering, degradation, and slope instability processes.

2.1 Field Surveys and Geotechnical Analysis

Field surveys were aimed at identifying stratigraphic and structural elements representing predisposing factors for land sliding.

Geo-structural data were collected and analyzed with RocScience Dips © software (RocScience 2020) to detect the bedding planes and the main sets of discontinuities. Rock samples were collected in the field for laboratory geotechnical analyses to assess the main physical and mechanical parameters. The following laboratory tests were conducted according to (ISRM 1985): (1) tilt test, (2) point load test, and (3) real unit weight (hydrostatic weighing).

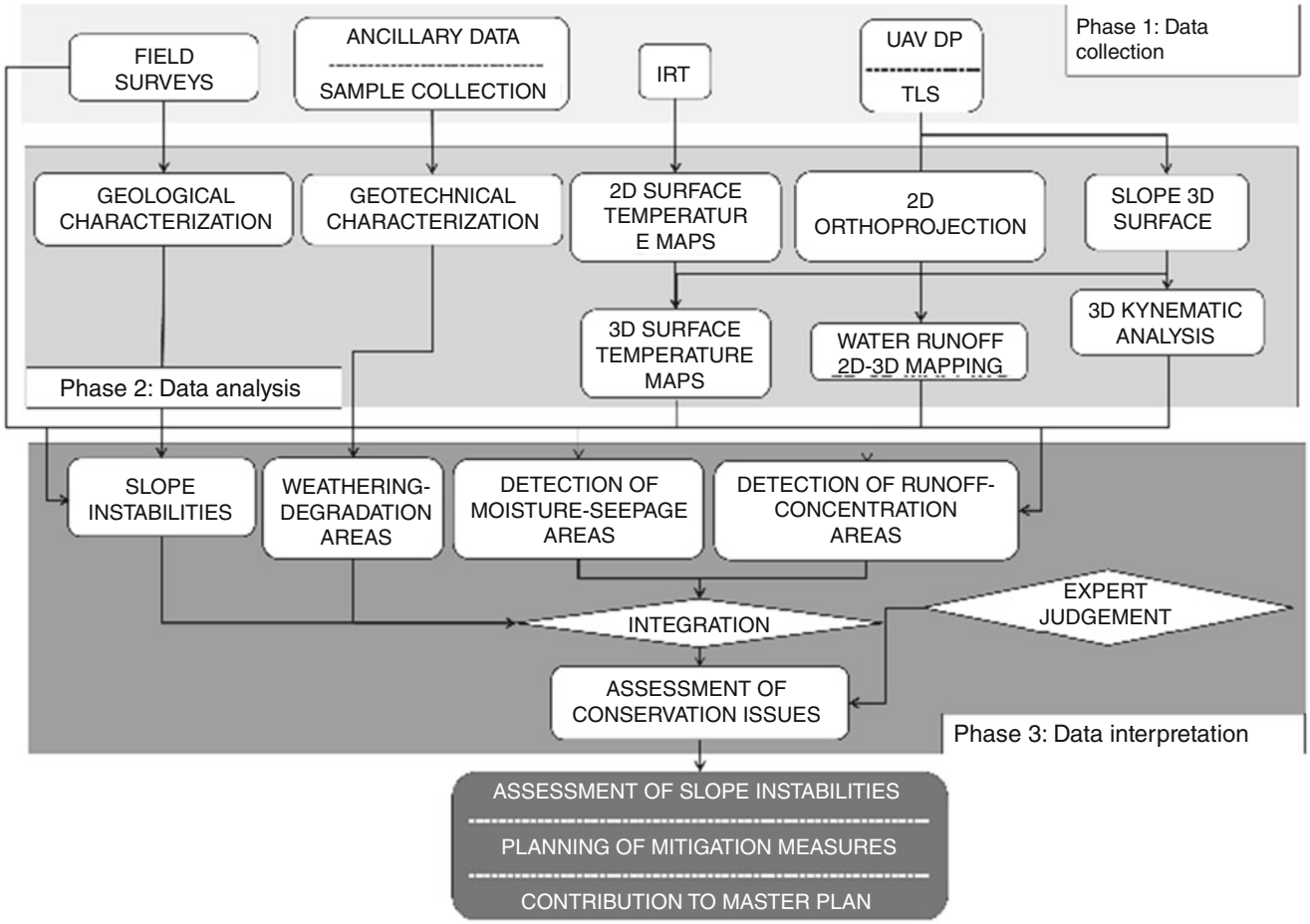

Fig. 2 Work plan of the adopted methodology

2.2 IRT Surveys

Calibrated thermal cameras are used in IRT for the detection and mapping of thermal radiation from the analyzed scenario (Nolesini et al. 2016; Frodella et al. 2017, 2020a, 2021). The IRT array detector acquires a digital image, called a "thermogram" or "thermographic image", which after a calibration procedure is converted by the built-in processor into a ST map (Spampinato et al. 2011).

The IRT surveys were performed with a hand-held FLIR SC620 model thermal camera (FLIR 2009), characterized by a focal plane array microbolometer sensor, a 640 × 480-pixel resolution, and a field of view of 24 × 18 degrees (see Table 1 for further specifications). The IRT surveys were carried out between July and November 2016 in Vardzia, while in the other sites in November 2018. During all the surveys, cloudy skies with low wind proved ideal conditions for the IRT surveys. Thermographic image mosaicking, correction and thermal focusing were carried out using FLIR Tools+ software (FLIR 2015).

2.3 DP-UAV Survey and Surface Runoff Modelling

Digital photogrammetry (DP) is a widely adopted and effective technique for acquiring 3D geometric data from stereoscopic overlaps of photo sequences captured by a calibrated digital camera (Chandler 1999). This technique can provide, in a short time, a detailed spatial representation for the analysis of the geometrical-structural setting and the surface changes of both ground and structures (Zhang et al. 2004). In the past few years, thanks to the rapid techno-logical development of digital cameras and low-cost and small Unmanned Aerial Vehicles (UAV), DP led to new, promising scenarios in cultural heritage applications (Grün et al. 2002; Bolognesi et al. 2014).

UAV-DP surveys were carried out in the analyzed sites with a DJI Phantom 4Pro quadcopter. Agisoft Photoscan software (Agisoft Photoscan 2017) was used for data processing and high-resolution Digital Terrain Model (DTM) construction. Ground control points were fixed using Differential Global Positioning System (DGPS), or

Table 1 IRT survey parameters of the analysed sites

Case study	Slope aspect	Sensor-target distance (m)	Image res. (cm)	Air T (C°) -Rh (%)
Vardzia	S	600	39	28.1;19.5 44.8;52.6
Vanis Kvabebi	W/E	100	6.6	14.4–63.4
Uplistsikhe	SW	100	6.6	21.3–33.6
Natlismcemeli	S	110/20	7.1/1.2	13.4–65.9
Sabereebi	SW	100/20	6.5	22.6–39.8

Table 2 Average values of the collected samples

Case study	Friction angle (°)	Uniaxial compressive strenght (MPa)	Unit weight (KN/m^3)
Vanis Kvabebi	28	2.70	16.76
Uplistsikhe	40	3.55	19.5
Natlismcemeli	27	0.49	16.56
Sabereebi	23	0.52	15.09

Total Station devices to increase the quality of the DTMs. ArcMap (ESRI) Hydrology Tools package was applied using Flow Direction, Accumulation and Stream Order functions to analyze the slope scale drainage system (ESRI 2019). This allowed us to model surficial water runoff trajectories, calculate the corresponding watersheds and categorize the stream order on the DTM.

3 Results

3.1 Geotechnical Data

The laboratory analysis of the samples in Vardzia showed generally high values of primary porosity for the four analyzed layers ($16 < n < 29$). In contrast, the higher values correspond to the tuff layers (with special regard to Layer 3). Also, rock moisture shows higher values in the tuff layers (up to 3.6 in Layer 2 and 3.5 in Layer 3, respectively), while in the volcanic breccia layers, it ranges from 0.6 to 2.6. All these values decrease with depth, showing the action of water infiltration on the weathering from the slope surface (on the contrary, the density increases in depth, as rock gets less weathered). The uniaxial compressive strength UCS for Layer 2 is equal to 9.3 MPa in dry conditions and 2.6 MPa in wet conditions, indicating a strong influence of water content on the material response. A similar effect was detected for the tensile strength σt estimated by the Brazilian tests (925 kPa in dry conditions and 300 kPa in wet conditions). Layer 3 is characterized by very similar physical and mechanical properties. The properties of Layer 1 were investigated by a limited number of tests: point load tests gave an average UCS value of 14.8 MPa in dry conditions. The corresponding values of the cohesion for dry and wet conditions were then calculated from the corresponding UCS values. According to the X-ray phase mineralogical analysis results, the main primary minerals of the rocks are Andesine-Labradorite, Hornblend, Biotite, rare occurrence of quartz, and calcite. Rock-building minerals are cemented by an amorphous phase (volcanic glass). Ca-montmorillonite, occurring in various quantities in all the samples of Vardzia complex rocks, is mainly a product of volcanic glass alteration, while its quantity is determined by the intensity of alteration process. For the sites of Vanis Kvabebi, Uplistsikhe, and David Gareja, all the collected rock samples are characterized by very low strength parameters (many samples were easily broken even by hand), with special regard for the David Gareja samples, showing that these rocks are very weakly cemented (Frodella et al. 2021) (Table 2).

3.2 Field Surveys

3.2.1 Vardzia and Vanis Kvabebi

Two main sets of discontinuities are recognized at Vardzia: (i) high-angle joints dipping SE parallel to the slope face and (ii) subvertical joints oriented NW–SE. These intersect the bedding of the volcanoclastic units along the entire cliff, causing several instability phenomena, such as rock falls, topples, and wedge-planar failures (Cruden and Varnes 1996; Margottini et al. 2015; Boldini et al. 2018; Frodella et al. 2020a). In Vanis Kvabebi Besides the sub-horizontal layer bedding, three main subvertical joint sets were identified (Fig. 3): (1) J1: dipping W and N-S oriented, forming the main slope faces (Fig. 6d); (2) J2: dipping NW and SW-NE oriented, it is responsible for the formation of a master joint intersecting all the upper sections on the eastern rock wall of the complex; (3) J3: dipping SE and trending NW-SE, it represents persistent fractures along which ephemeral creek erosion has caused deep channel cuts in the southern sector of the complex.

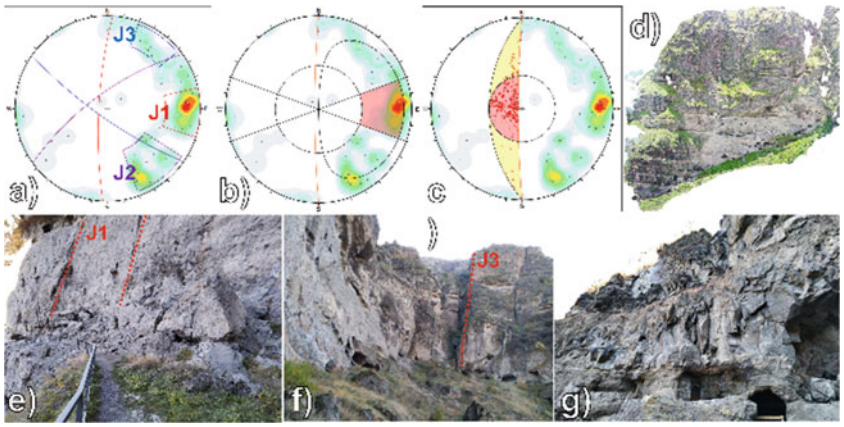

Fig. 3 Structural setting and kinematic analysis: identified sets (**a**); kinematic analysis for planar (**b**) and wedge (**c**) failure; frontal view of the rock cliff from UAV-DP (**d**); 2017 rock fall deposits (**e**); subvertical fracture where creek channel erosion has concentrated (**f**); welded tuff portion affected by wedge failures (**g**)

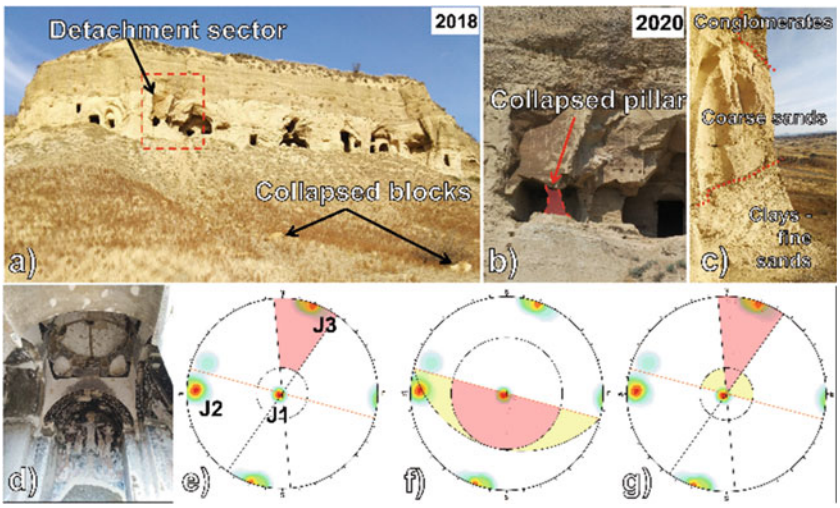

Fig. 4 2D kinematic analysis: Wedge failure mechanism (**a**); Planar failure mechanism (**b**). Field evidence of kinematic mechanisms: wedge failure (**c**) and plane failure (**d**)

3.2.2 Uplistsikhe

Four main identified discontinuity sets were identified in the field: J1 (bedding) dips SE with low angles, J2 joint set dips SW parallel to the slope face with high angles, J3 is a subvertical joint set trending WNW-SSE, and J4 dips NW with mid-high angles (Frodella et al. 2021). The 2D kinematic analysis highlighted two equally predominant instability mechanisms: plane and wedge failures.

3.2.3 David Gareja

In Natlismcemeni the main discontinuities are organized in two main joint sets: J1 is related to the bedding and dips NE against the slope with low angles; J2 is a mainly subvertical set dipping SW along the slope; J3 is a subvertical fracture sparsely cutting the cliff face (Fig. 4) (Frodella et al. 2021).

The performed 2D kinematic analysis allowed us to assess the main instability mechanisms affecting the rock cliff, which are represented by plane failure, followed by wedge failure, and subordinately by toppling and free fall. The latter can be locally predominant in overhanging sectors, such as cave niches, while open fractures parallel to the slope can develop topplings. Very persistent and spaced wide-open fractures enhancing are visible within the monastery caves and can potentially seriously damage the complex.

In Sabereebi, the bedding (J1) dips NE towards the slope with low angles, while two not widely spaced but persistent discontinuity sets cut the slope parallel (J2) and orthogonal (J3) to the cliff face, dipping E and SSW respectively, deeply controlling the stability of the cliff. The 2D kinematic analysis confirms high planar and especially wedge failure indexes along these planes, subordinately toppling.

3.3 Remote Sensing Analysis

3.3.1 Vardzia

The IRT data (Fig. 5) shows lower surface temperatures (ST) in the upper slope sectors (mean value: 23.2 °C during S1 = July and 11.1 °C during S2 = November) than in the lower slope sectors, likely due to the widespread vegetation cover of the former.

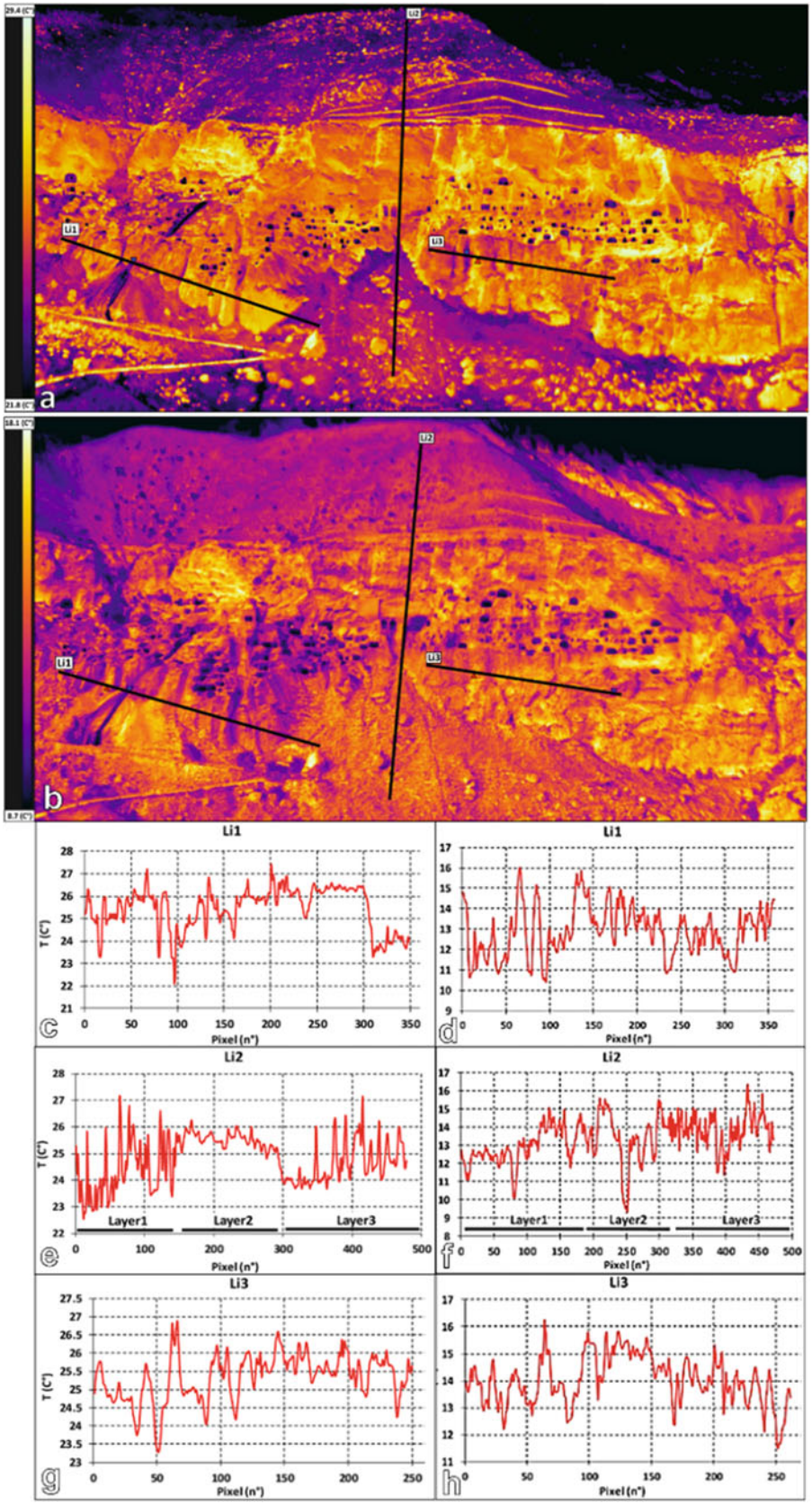

Fig. 5 Vardzia IRT data: (**a**) Mosaicked thermograms acquired on July 16th, 2016, at 19:00 (**a**), on November 20th at 18:40 (**b**). Surface temperature profiles Li1–3 from the IRT data in a (**c**, **e**, **g**) and **b** (**d**, **f**, **h**) (modified after Frodella et al. 2020a)

Some minor warm temperature anomalies (up to 29.4 °C during S1 and 14.7 °C in S2) were observed corresponding to the scattered boulders of the upper breccia, which are isolated from the surrounding finer matrix due to differential erosion. Another widespread vegetated sector is the slope toe, showing slightly higher mean ST values (mean value: 24.1 °C during S1 and 13.4 °C during S2) than the upper slope. Warm temperature anomalies were also detected (up to 29.7 °C during S1 and 17.9 °C) in association with the presence of fallen block deposits that were, in turn, associated with rock cliff face instabilities. The rock cliff shows the highest ST values in the thermal image (mean of 27.8 °C during S1 and 14.1 °C during S2), although several cold thermal anomalies are also present. Based on their spatial patterns, their locations, and interpretation of the corresponding visible-light images, these temperature anomalies can be described as follows: (i) a cave system carved in Levels 2 and 3 (mean ST of 21.1 °C during S1 and 8.9 °C during S2); (ii) vegetated sectors located on both the eastern and western edges (22 °C mean ST during S1 and 9.6 °C during S2); and (iii) near-linear, subvertical anomalies intersecting (21.6 °C mean ST during S1 and 10.2 °C during S2). These subvertical anomalies were detected in both surveys corresponding with open, persistent, subvertical fracture systems orthogonal to the cliff face, that intersect nearly all the layers. Considering their spatial pattern and the continuous rainfall before both surveys, these anomalies were interpreted as moisture areas associated with ephemeral drainage networks. In particular the sharpest of these anomalies, along a slope debris talus, was associated with seepage from a water pipe used for excavation purposes by the local group of archaeologists. Additional cold thermal anomalies were located within the slope toe sector, mostly along the contact of the slope toe with the cliff face; other anomalies exhibited vertical linear shapes representing minor rills.

The hydromodelling allowed us to map the spatial distribution of water runoff within the monastery complex of Vardzia, confirming the insights from the IRT analysis. Streams were categorized by order, and catchments and areas of concentration were identified (Fig. 6). Results of the 2D ortho-projection showed three main catchments in the eastern sector (Streams 1–3) and one located at the western edge of the complex (Stream 4), each showing streams up to the fifth order. At the top of the central slope sector, the hydromodelling showed the effect of runnels and retaining walls on the water runoff. In fact, the runnels effectively channel minor streams toward the two adjacent main-order catchments to the west and the east. However, in some sectors, these runnels have been damaged by the impacts of detached boulders from the uppermost slope sector, so water flows directly along the slope at some points.

The 3D model provides a clear frontal view of the water runoff patterns on the cliff face and on the slope toe (Fig. 6). Four areas of water concentration are present at the slope break between the upper slope and cliff. These are key sites of water runoff concentration, acting as areas of linear erosion, especially in association with Layer 1. From the slope 3D model, it is also evident how the slope morpho-structural setting in the middle–lower cliff sector creates other areas of interest concerning water concentration along large, eroded fractures.

3.3.2 Vanis Kvabebi

In Vanis Kvabebi, the IRT surveys allowed mapping the whole cliff face, highlighting dry conditions corresponding to the collapsed sector. The integrated analysis allowed the detection of other potentially unstable sectors represented by warm thermal anomalies highlighting open-cavernous features (over one meter of fracture aperture; ISRM 1978). These are located along a persistent J2 system master joint intersecting all the basalt flows, which in turn creates a niche at the contact with the underlying more erodible medium-grained tuffs (Fig. 3) (Frodella et al. 2021).

Dry conditions were assessed in the 2017 collapse area (Fig. 7). In the cliff's southern sector, the IRT analysis showed the presence of cold thermal anomalies along the erosional channels developed along the J3 joint system, suggesting the presence of moisture areas (Fig. 7). These warm thermal anomalies also highlight the widespread niches in open features associated with J1 fractures. The hydro-model showed that very low-order ephemeral streams concentrate within J3 fractures within the collapse area. The same discontinuity system is responsible for the water runoff concentration in the slope's southern sector, where streams up to the fifth order are located (Fig. 7). Here, runoff concentrates within wide master joints, generating wide erosional channels cutting deeply into the cliff, as also highlighted by the IRT analysis.

3.3.3 Uplistsikhe

The IRT survey highlighted warm thermal anomalies along persistent joints belonging to J4, where minor rock falls occurred in 2019 (Fig. 8). General dry conditions were assessed along the rock cliff except for the left sector, where a cold thermal anomaly (as well as the presence of vegetation and weathering coating) reveals the presence of an ephemeral stream, which concentrates along J4, the rock cliff most persistent discontinuity set (Fig. 8).

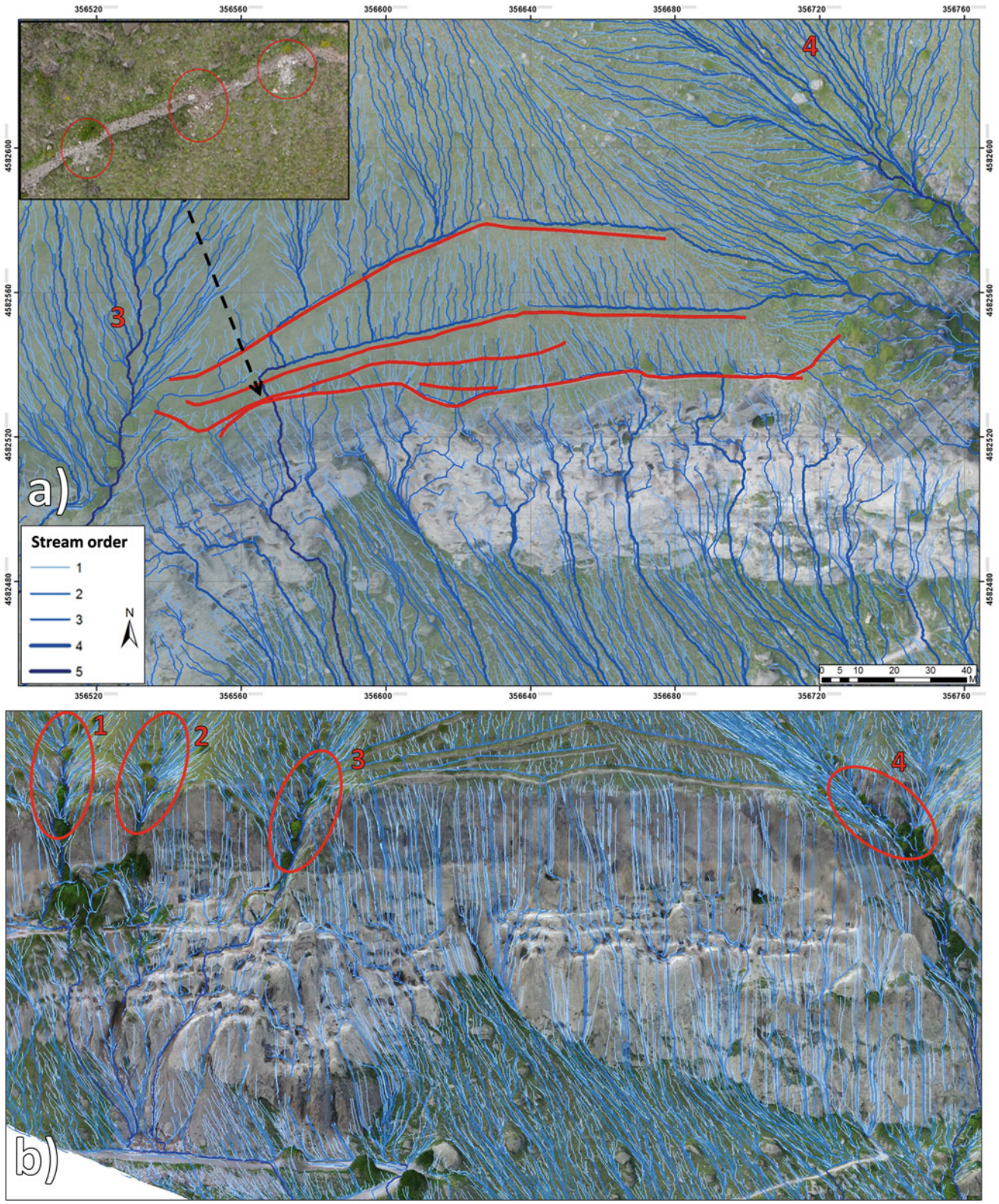

Fig. 6 Unmanned aerial vehicle digital photogrammetry (UAV-DP) products: (**a**) two-dimensional (2D) orthoprojection of Vardzia's hydrographic network on the upper slope sector and cliff face; (**b**) Modeled drainage network for the Vardzia slope's three-dimensional (3D) surface (modified after Frodella et al. 2020a)

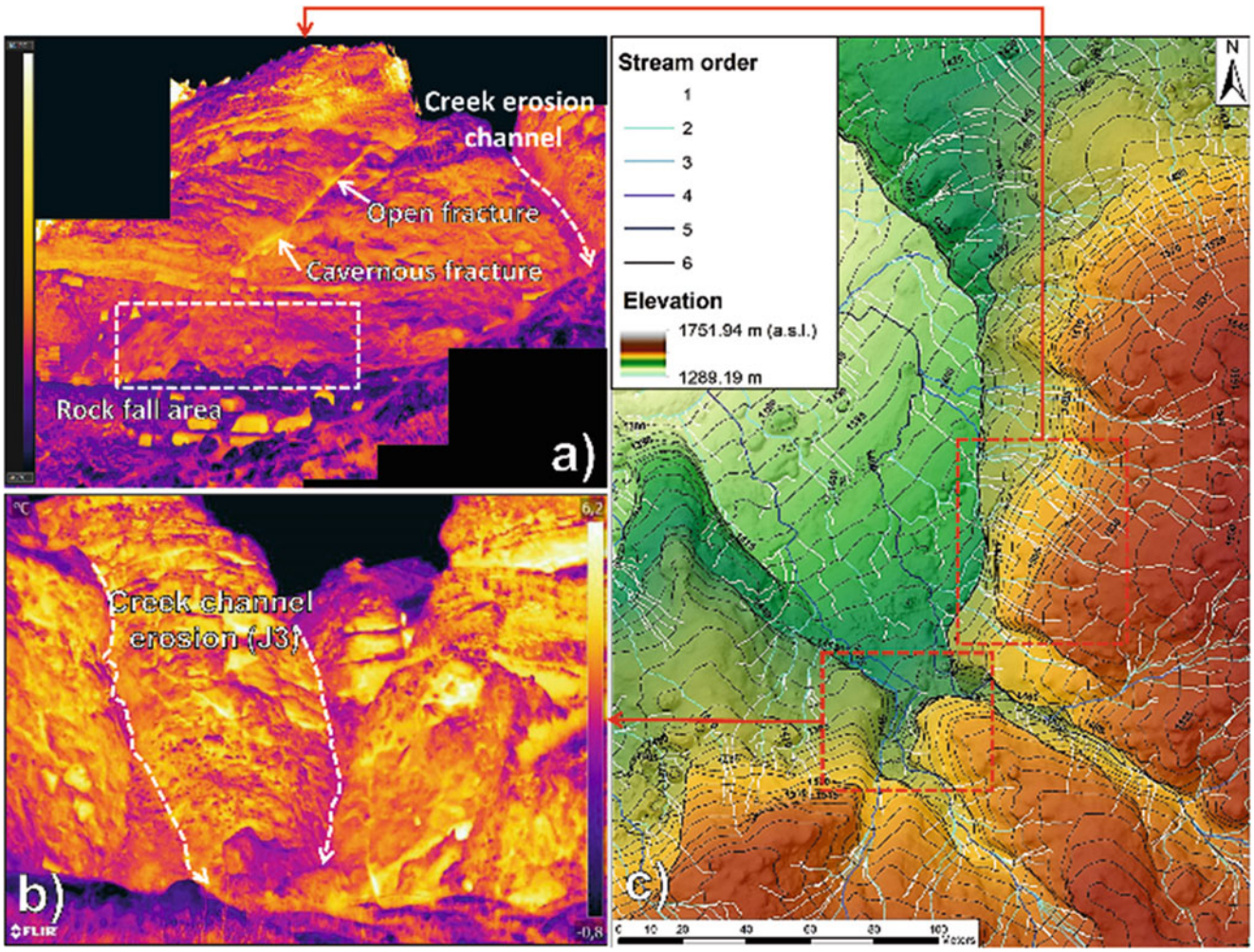

Fig. 7 Vanis Kvabebi IRT data: western main cliff (**a**), and southern rock wall (**b**). Drainage network map (dashed red squares represent areas of interest) (**c**)

This is also confirmed by the hydro-modelling analysis (red arrow in Fig. 8), which also shows how the high-order ephemeral streams concentrate mainly along J3-J2 sets, while low-order ephemeral streams are mainly along J4.

3.3.4 David Gareja

The IRT surveys in Natlismcemeni pointed out that while the rock slope shows average values between 10.2–10.8 C°, warm thermal anomalies (13.8–14.1 C°) were detected both at the top of the thick sandy layer (herein related to J1) and at the topmost sector of the caved accesses, highlighting potentially unstable ledge-niche systems (Fig. 9). Warm thermal anomalies also enhance wide open fractures parallel to the slope (related to J2; Fig. 9). No cold thermal anomalies were detected, therefore dry conditions were assessed. In Sabereebi, IRT analysis showed average temperatures of 26.8 °C of the slope face and warm thermal anomalies (from 31 to 42 C°) in correspondence with the recent collapse sector and the underlying slope talus, where erosion is exposing bare soil (Fig. 10). Sharp cold thermal anomalies (15.4–17.7 °C) highlight a large system of open cracks connected to J3 at the right end of the complex (Fig. 10). As for Natlismcemeni, dry conditions were assessed. The UAV-DP survey and the Hydro-modelling analysis provided a high-resolution DEM, and drainage maps (Fig. 10). This latter showed main cataclinal-type streams draining the hogback of the monoclinal structure to the NE.

In contrast, small anaclinal-type streams erode the debris talus underlying the monastery (as shown by the bare soil sectors highlighted by IRT). This phenomenon could gradually undermine the stability of the cliff.

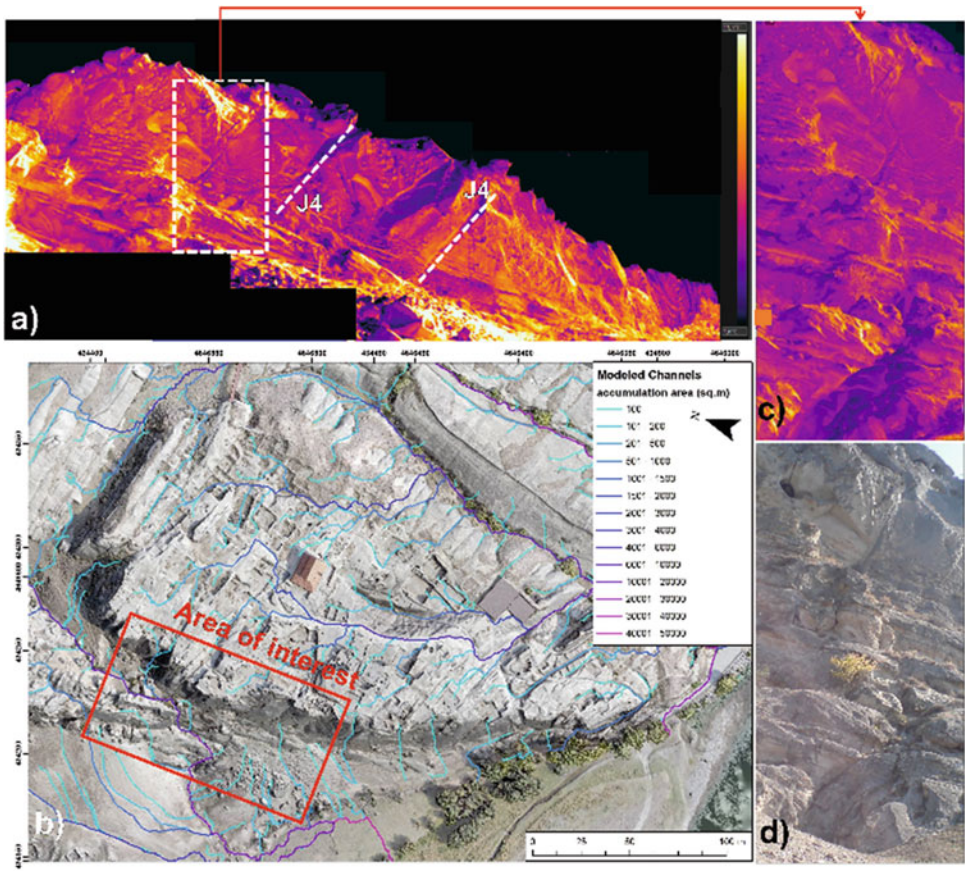

Fig. 8 IRT data of the Uplistsikhe western cliff (mosaicked thermograms with 2800 × 850 pixel) (**a**); modelled ephemeral drainage network of the site (**b**); ephemeral stream IRT and optical image (**c**, **d**), developing along J4 fracture (white dashed rectangle in a)

4 Discussion

In Vardzia, the stratigraphic position and the geomechanical properties of the volcanic breccias play important roles in the current geological structure of the complex. Since this stratum of breccias is located atop the tuffs, their higher density and hardness have protected the softer and weaker tuffs below from erosion (Margottini et al. 2015). Nevertheless, the breccias are currently being deeply cut by stream erosion across the slope's western sector. This phenomenon is responsible for the fast surface weathering of the rock

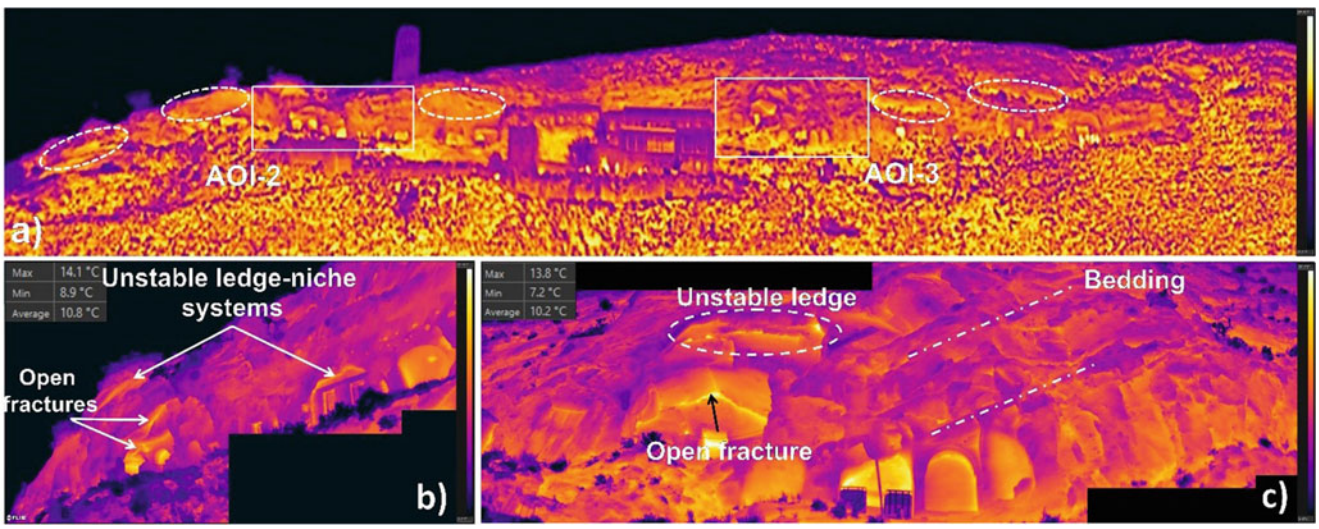

Fig. 9 Outcomes of the IRT surveys of the Natlismcemeni monastery: (**a**) IRT mosaicked image (2075 × 505 pixels with 7.1 cm) showing the AOIs and the warm thermal anomalies (dashed ovals); (**b**) 1160×480 pixels; (**c**) 2120 × 590 pixels

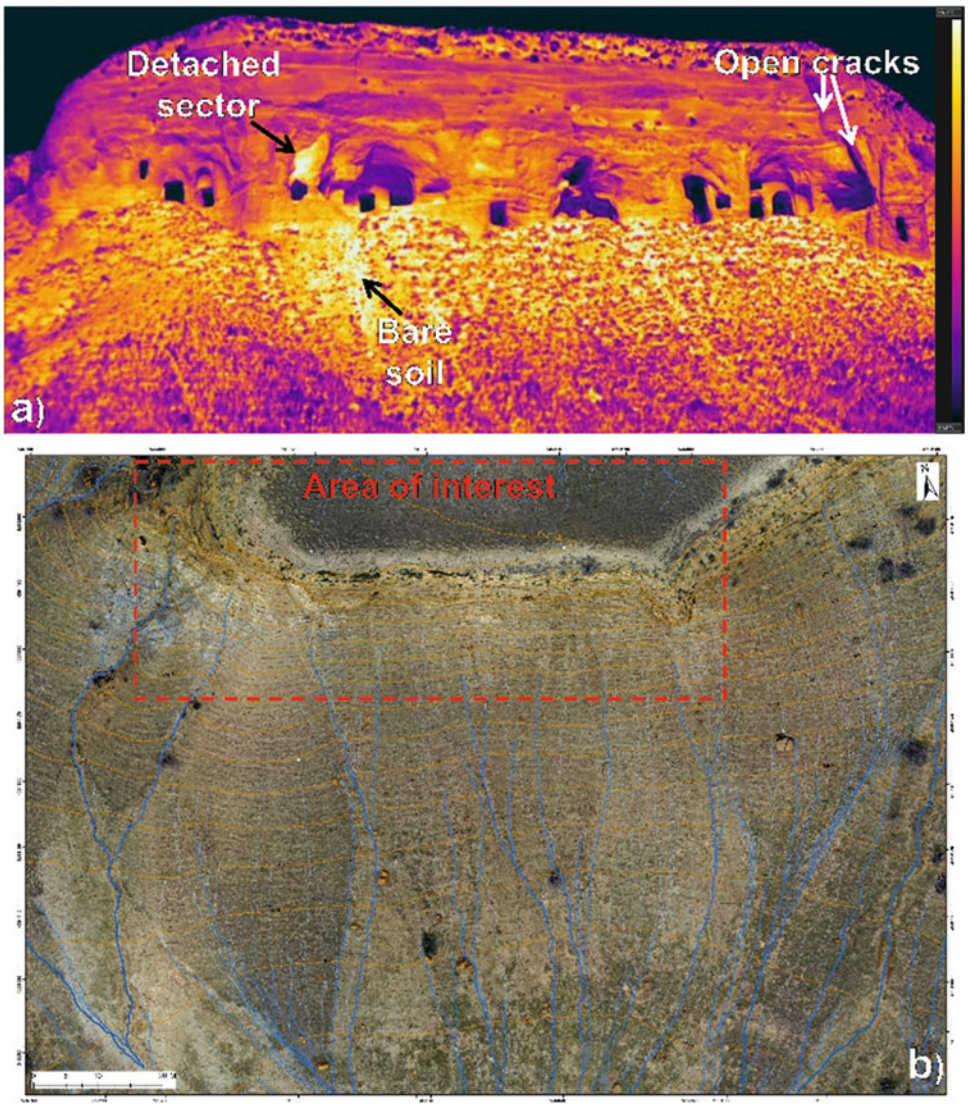

Fig. 10 IRT and UAV-DP data in Sabereebi: mosaicked surface temperature map (950 × 480 pixels with 6.5 cm resolution (**a**). UAV-DP high resolution DEM derived products: drainage pattern map (**b**)

mass. Furthermore, hygric expansion due to water runoff and concentration further exacerbates this scenario since it negatively affects both geotechnical properties and the strength of the discontinuities (Boldini et al. 2018). In Vardzia, the obtained ST maps allowed the mapping of the moisture patterns in correspondence with large subvertical open fractures; these constitute the main ephemeral streams developing along the slope. The association of ST anomalies with moisture demonstrates that the ephemeral drainage pattern is concentrated within the subvertical joint system affecting mostly Layers 1–4 in and 3–4. Rill erosion, in particular, involves the debris talus of the slope. The hydro-modeling analysis on the UAV-DP products confirmed the insights provided by IRT and provided an accurate mapping of the slope ephemeral drainage network. This represents areas of preferential surface erosion and weathering, mainly in Layers 2 and 3. These streams cause moderate mass transport and deposition at the slope toe, creating small taluses. In Vardzia, water runoff and moisture, which often occur in the tuff layers represent an important predisposing factor for instability phenomena.

To mitigate slope instability a new low-cost, low-impact system of runnels and retaining walls should be designed and implemented in the slope's western sector, together with filtering weirs within the creek bed rock cuts (Fig. 11).

In Vanis Kvabebi, the main conservation issues are the following: (i) linear erosion along persistent and open master joints; (ii) slope instabilities due to the combination of the stratigraphy (soft erodible ash layers alternating with tuff layers) and the structural setting. These, in particular, create several unstable protruding and overhanging sectors along the slope. The most relevant instabilities are represented by wedge failure and plane failure. The latter can be locally predominant in overhanging sectors, such as that affected by the 2017 collapse. The adopted methodology supplied insights into the influence of the fracture system with respect

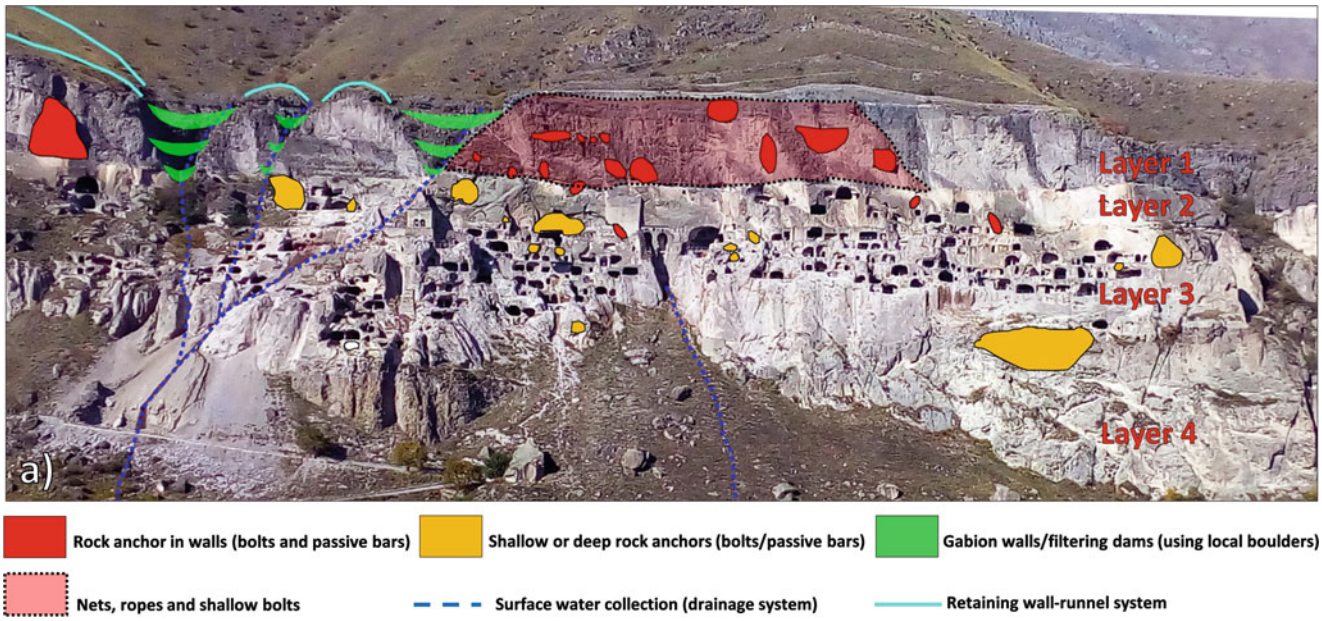

Fig. 11 General master plan for the proposed mitigation measures for the whole Vardzia Monastery

to the hydraulic setting. The collected information was then used as a fundamental input for framing conservation strategies. Furthermore, accurate mapping of open fractures provides useful information for planning a crack meter network for monitoring local deformation. The UAV-DP orthoprojection image granted a useful topographic reference to be used as a starting point for the planning of future conservation works (Fig. 12).

In Uplistsikhe, several critical areas were selected, among which the rockfall-affected areas were selected as the highest priority for the consolidation works. These started from Area 1 by reinforcement of a critical block on the rock cliff using of deep anchoring. A special hanging scaffolding was constructed and fifteen horizontal drillings to depths up to 9 meters were conducted, where the still anchors were fixed and cemented. A water-diverting structure will also be planned in correspondence with the ephemeral stream highlighted in Fig. 8. This first stage of mitigation works will enable the opening of the historical entrance into the Uplistsikhe rock town, located at the bottom of the rock cliff.

In David Gareja, there is generally not a predominant instability process acting in the analyzed sites: they can all be reconducted to rock collapses directly dependent on local structural settings differently interacting with the slope face and stress release. In Natlismcemeni, the performed activities proved to be effective tools in enhancing potentially unstable ledge-niche systems and open fractures, and defining the more landslide-prone sectors as priority areas for sealing/reinforcement.

In Sabereebi, erosional processes caused by an ephemeral stream in the debris talus can undermine the stability of monastery pillars. Future mitigation works to be planned are drainage channels to avoid overland flow on top of the rock slope and erosion of the underlying debris talus. Non-structural mitigation actions, such as the implementation of a monitoring system for the measurement of displacements, such as robotized topographic stations and Ground-based Synthetic Aperture Radar systems, are being implemented. Such action is important for locating the priorities in the areas of intervention, in the framework of the site's preservation, as well as for the safety of local monks, for the staff of rock-climbers which will be operating in reinforcement/conservational tasks in the next future, and for visiting tourists.

5 Conclusions

In all the analyzed sites, the field surveys provided fundamental insights into the acting erosion, weathering, and instability processes affecting the rock cliffs of both sites. Meanwhile, the remote sensing approach provided full coverage of the analyzed slopes, allowing for the detection of slope criticalities in inaccessible or hazardous sectors while granting the safety of the operators. The portability, fast acquisition, and processing times of IRT were profitably applied at both sites for a preliminary mapping of the slope surface moisture sectors associated with ephemeral drainage networks. At the same time, UAV-DP high-resolution

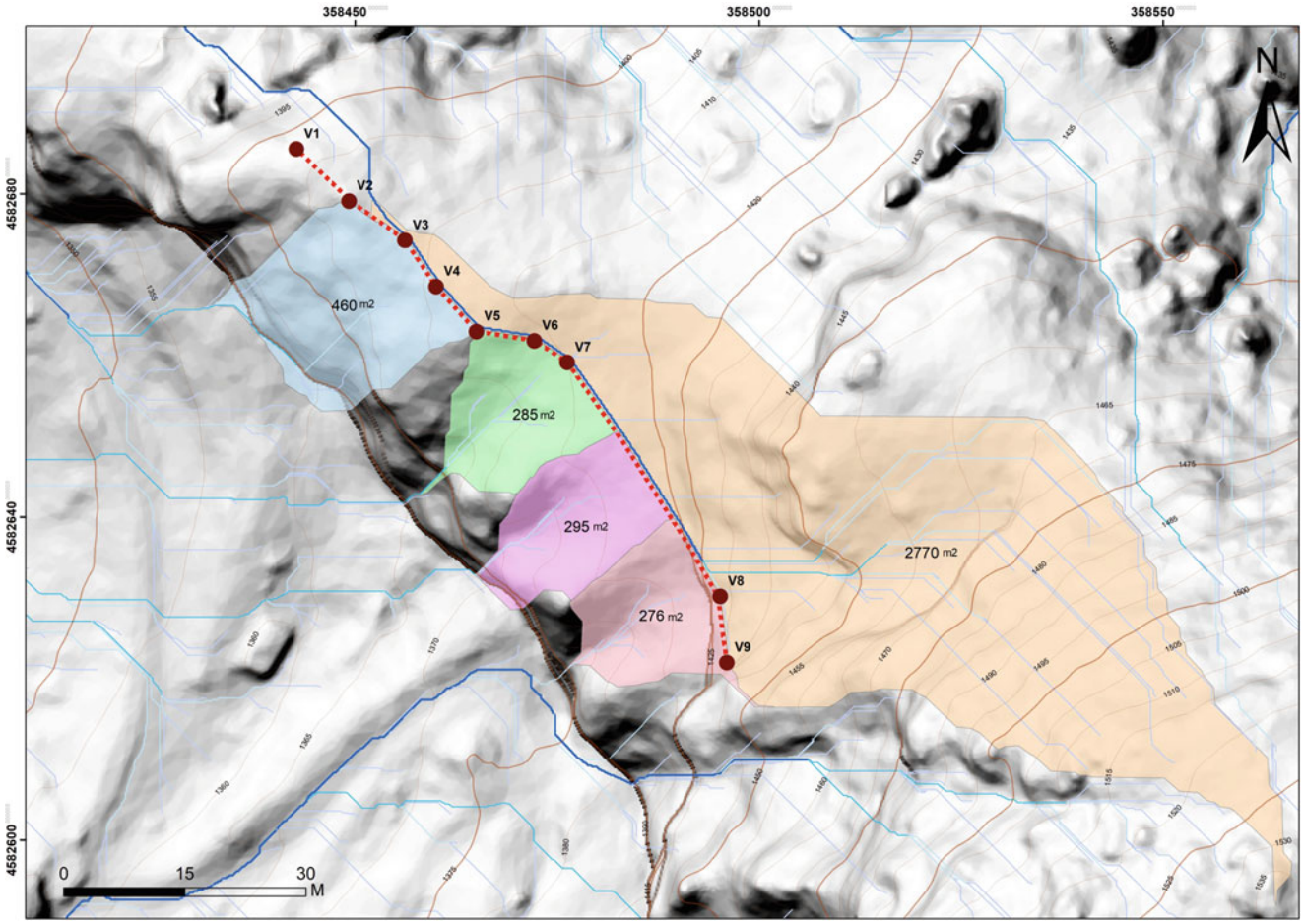

Fig. 12 Hydrographic model of Vanis Kvabebi western cliff showing the watershed surfaces, the area where the water drainage system is planned (the red dashed line shows the planned water diverting wall)

surfaces were useful for performing with high accuracy the hydro-modeling. Generally, the detected ephemeral stream pattern is controlled by the morphological interaction with the main rock slope fractures. This approach served as the basis for proposing the implementation of new drainage channels and retaining walls. Given the possible logistical limitations in the planning of an IRT survey, the timing of the survey and the position of the thermal camera must be carefully considered to obtain both the best image resolution and the widest field of view of the scenario at the same time avoiding the shadowing effects on the slope. Future advancements should include the application of fixed thermal camera installations in remote surveying and monitoring stations for gathering continuous, high-resolution, real-time IRT data. A skilled thermal camera operator is strongly recommended for correct IRT image acquisition, elaboration, and interpretation procedures.

Acknowledgments This work was carried out in the framework of a Bilateral agreement between the Earth Science Department of the University of Florence (Italy) and the Faculty of Natural Sciences and Engineering of Ilia State University (Tbilisi, Georgia). The authors are very grateful to the National Agency for Cultural Heritage Preservation of Georgia (NACHPG) and to all the staff members for their support in the present research.

References

Agisoft Photoscan (2017) datasheet. https://www.agisoft.com/pdf/photoscan-pro_1_4_en.pdf. Last Access December 2019

Boldini D, Guido GL, Margottini C, Spizzichino D (2018) Stability analysis of a large-volume block in the historical rock-cut city of Vardzia (Georgia). Rock Mech Rock Eng 51(1):341–349

Bolognesi M, Furini A, Russo V, Pellegrinelli A, Russo P (2014) Accuracy of cultural heritage 3D models by RPAS and terrestrial photogrammetry. The International Archives of Photogrammetry, Remote Sensing and Spatial Information Sciences 40(5):113–119

Chandler J (1999) Effective application of automated digital photogrammetry for geomorphological research. Earth Surf Process Landf 24: 51–63

Cruden DM, Varnes DJ (1996) Landslide types and processes. In: Turner AK, Schuster RL (eds) Landslides investigation and

mitigation, 1996, special report 247. Transportation Research Board, Washington, D.C, pp 36–75

ESRI (2019) ArcMap 10.6 datasheet. ESRI Inc. https://www.esri.com/content/dam/esrisites/en-us/media/pdf/product/desktop/ArcGIS-10.6-Desktop-ArcMap-Functionality-Matrix.pdf. Last Access October 2019

FLIR (2009) FLIR ThermaCAM SC620 technical specifications. FLIR systems Inc. www.flir.com/cs/emea/en/view/?id=41965. Last Access July 2019

FLIR (2015) FLIR tools+ datasheet. FLIR systems Inc. https://www.infraredcamerawarehouse.com/content/FLIR%20Datasheets/FLIR%20ToolsPlus%20Datasheet.pdf. Last Access September 2019

Frodella W, Gigli G, Morelli S, Lombardi L, Casagli N (2017) Landslide mapping and characterization through infrared thermography (IRT): suggestions for a methodological approach from some case studies. Remote Sens 9(12):1281

Frodella W, Elashvili M, Spizzichino D, Gigli G, Adikashvili L, Vacheishvili N, Kirkitadze G, Nadaraia A, Margottini C, Casagli N (2020a) Combining InfraRed thermography and UAV digital photogrammetry for the protection and conservation of rupestrian cultural heritage sites in Georgia: a methodological application. Remote Sens 12(5):892

Frodella W, Spizzichino D, Gigli G, Elashvili M, Margottini C, Villa A, Frattini P, Crosta G, Casagli N (2020b) Integrating kinematic analysis and infrared thermography for instability processes assessment in the rupestrian monastery complex of David Gareja (Georgia). Understanding and reducing landslide disaster risk. Springer, Cham, pp 457–463

Frodella W, Elashvili M, Spizzichino D, Gigli G, Nadaraia A, Kirkitadze G, Adikashvili L, Margottini C, Antidze NC, N. (2021) Applying close range non-destructive techniques for the detection of conservation problems in rock-carved cultural heritage sites. Remote Sens 13:1040

Grün A, Remondino F, Zhang L (2002) Reconstruction of the great Buddha of Bamiyan, Afghanistan. Int Arch Photogramm Remote Sens 34(5):363–368

Gudjabidze GE, Gamkrelidze IP (2003) Geological map of Georgia 1: 500 000. Georgian State Department of Geology and National Oil Company "Saqnavtobi"

ISRM (1978) Suggested methods for the quantitative description of discontinuities in rock masses. Int J Rock Mech Min Sci Geomech Abs 15(6):319–368

ISRM (1985) Suggested methods for determining point load strength. Int J Rock Mech Min Sci Geomech, Abs 22(2):51–62

Margottini C, Antidze N, Corominas J, Crosta GB, Frattini P, Gigli G, Giordan D, Iwasaky I, Lollino G, Manconi A, Marinos P, Scavia C, Sonnessa A, Spizzichino D, Vacheishvili N (2015) Landslide hazard, monitoring and conservation strategy for the safeguard of Vardzia byzantine monastery complex. Georgia Landslides 12(1): 193–204

Nolesini T, Frodella W, Bianchini S, Casagli N (2016) Detecting slope and urban potential unstable areas by means of multi-platform remote sensing techniques: the Volterra (Italy) case study. Remote Sens 8(9):746

Okrostsvaridze A, Popkhadze N, Bluashvili D, Chang YH, Skhirtladze I (2016) Pliocene Quaternary Samtskhe-Javakheti Volcanic Highland, Lesser Caucasus, as a result of mantle plumes activity. In: Gilbert, A. S., and Yanko-Hombach, Valentina, eds., Proceedings of the Fourth Plenary Conference of IGCP 610 "From the Caspian to Mediterranean: Environmental Change and Human Response during the Quaternary (October 2–9, 2016; Tbilisi, Georgia)". Georgian National Academy of Sciences, Tbilisi, pp 127–131

Rocscience (2020) Dips. v8 graphical and statistical analysis of orientation data. Rocscience Inc., Toronto, Ontario

Spampinato L, Calvari S, Oppenheimer C, Boschi E (2011) Volcano surveillance using infrared cameras. Earth Sci Rev 106:63–91

Stinghen A (2011) Tectonic and geomorphological evolution of the kartalini basin, Georgia, University of Padua, Master's thesis in Geology, p 109

Zhang Z, Zheng S, Zhan Z (2004) Digital terrestrial photogrammetry with photo total station. International Archives of Photogrammetry and Remote Sensing, Istanbul, pp 232–236